# Supporting Information for "Assimilation of both column- and layer-integrated dust opacity observations in the Martian atmosphere"

Tao Ruan[1], R. M. B. Young[1,2], S. R. Lewis[3], L. Montabone[1,4],

A. Valeanu[1]and P. L. Read[1]

[1]Atmospheric, Oceanic and Planetary Physics, Department of Physics, University of Oxford, Clarendon Laboratory, Parks Road, Oxford, OX1 3PU, UK

[2]Department of Physics & National Space Science and Technology Center, UAE University, Al Ain, United Arab Emirates

[3]School of Physical Sciences, The Open University, Walton Hall, Milton Keynes, MK7 6AA, UK

[4]Space Science Institute, Boulder, CO 80301, USA

## Contents of this file



**Introduction** In the following three sections we include additional figures that supplement the information provided in the main text. Section S1 presents additional figures showing the performance of the reanalyses against in-sample observations. Section S2 presents additional figures that provide in-depth comparisons between various climatolog-

ical fields from the reanalysis and diagnostics obtained from the Mars Climate Database version 5.2.

**S1. Verification against in-sample observations**

The methods described in the main text were used to analyse various combinations of THEMIS and MCS observations obtained during Mars Years 28 and 29, representing a typical pair of years that include dusty seasons both with and without a planet encircling event. In this section we present results that evaluate the convergence of the assimilation towards the input data.

The model temperatures (either from the free-running model or the assimilated model state) were interpolated to the temperature retrieval pressure levels, before being converted to a global mean difference between model and observations. Figure S1 shows this difference averaged over several pseudo-height ranges (0–10 km, 10–20 km, 20–30 km, 30–40 km, and 40–80 km), assuming a 10 km scale height and a 610 Pa surface pressure. MCS retrievals are reported at pressure levels separated by around 1–1.5 km, while the true instrumental resolution is about 5 km (Kleinböhl et al., 2009), so this grouping of vertical levels smoothes the oversampled MCS retrievals over a distance larger than the true observational vertical resolution. Figure S2(a,b) shows the correlation between the assimilated THEMIS observations and the CIDO-only reanalysis and free-running model. Figure S3 shows the global-time mean difference in dust opacity between the in-sample observations and both the reanalysis and free-running model (see main text).

## S2. Contrasting interpolation of dust observations with assimilation

The earliest attempts to assimilate observations of column integrated dust optical depths simply collated these observations during short interval (usually around 1 sol) and interpolated them onto the model grid, using relatively broad point spread functions in the horizontal and a prescribed profile in the vertical, to obtain an estimate of the dust distribution during that interval (Lewis et al., 2007; Montabone et al., 2014). No attempt was made to transport the dust in a physically consistent manner using the modelled winds. This is the method used, for example, to produce the first MACDA reanalysis (Montabone et al., 2014), during which the dust distribution was held constant until new observations became available to enable the distribution to evolve in time. This prescribed dust distribution was then used as input to the model radiative transfer scheme in an attempt to correct the solar heating rate towards a more realistic distribution.

Figure S4 illustrates an example of this method during a "flushing" regional dust storm that occurred during the period assimilated during the present study, showing daily dust fields obtained from MCS column integrated optical depths by Montabone et al. (2015) for their dust scenario reconstructions and available online from `http://www-mars.lmd.jussieu.fr/mars/dust_climatology/index.html`. These show the movement of a dust cloud from the northern hemisphere into the south, where it grows and develops into a more substantial event near the Hellas Basin before spreading further south. Figure S5 shows the same period as represented in the present reanalysis using combined THEMIS CIDO-MCS LIDO observations assimilated into a model that advects and transports the dust tracer. Both figures show a broadly similar evolution of the storm during this period, but the interpolated dust cloud in Fig. S4 is much noisier with clear evidence

of modulation by the orbital pattern of the MRO spacecraft on a scale of around 15° longitude. The dust clouds in the assimilated reconstruction of this event are significantly smoother with better consistency between daily mean maps. Further details of this case will be presented by Ruan et al. (2022, in preparation).

**S3. Reanalysis vs. MCD comparisons** Figures S8–S17 contain the complete set of comparisons made between the reanalysis and the Mars Climate Database. The following quantities are included: surface temperature (Figs S6-S7), surface pressure (Figs S8-S9), atmospheric temperature (Figs S10-S11), density (Figs S12-S13), zonal velocity (Figs S14-S15), and meridional velocity (Figs S16-S17).

Surface quantities are monthly means (i.e. over 30 $L_s$) and atmospheric quantities are zonal-monthly means. Comparisons are made each month between MY28 $L_s = 120 - 150°$ and MY29 $L_s = 330 - 360°$ (20 months in total). Each plot shows the reanalysis monthly mean, MCD monthly mean, monthly mean difference (reanalysis minus MCD), reanalysis day-to-day variability, MCD day-to-day variability, and day-to-day variability ratio (reanalysis : MCD). The layout and format of each figure is the same.

## References

Kleinböhl, A., Schofield, J. T., Kass, D. M., Abdou, W. A., Backus, C. R., Sen, B., ... McCleese, D. J. (2009). Mars Climate Sounder limb profile retrieval of atmospheric temperature, pressure, and dust and water ice opacity. *J. Geophys. Res.*, *114*(10), E10006. doi: 10.1029/2009JE003358

Lewis, S. R., Read, P. L., Conrath, B. J., Pearl, J. C., & Smith, M. D. (2007). Assimilation of thermal emission spectrometer atmospheric data during the Mars Global Surveyor aerobraking period. *Icarus*, *192*(August), 327–347. Retrieved from `http://www`

.sciencedirect.com/science/article/pii/S0019103507003557 doi: 10.1016/j.icarus.2007.08.009

Montabone, L., Forget, F., Millour, E., Wilson, R. J., Lewis, S. R., Cantor, B., ... Wolff, M. J. (2015). Eight-year climatology of dust optical depth on Mars. *Icarus*, *251*, 65–95. Retrieved from http://dx.doi.org/10.1016/j.icarus.2014.12.034 doi: 10.1016/j.icarus.2014.12.034

Montabone, L., Marsh, K., Lewis, S. R., Read, P. L., Smith, M. D., Holmes, J., ... Pamment, A. (2014). The Mars Analysis Correction Data Assimilation (MACDA) Dataset V1.0. *Geoscience Data Journal*, *1*(2), 129–139. Retrieved from http://dx.doi.org/10.1002/gdj3.13 doi: 10.1002/gdj3.13

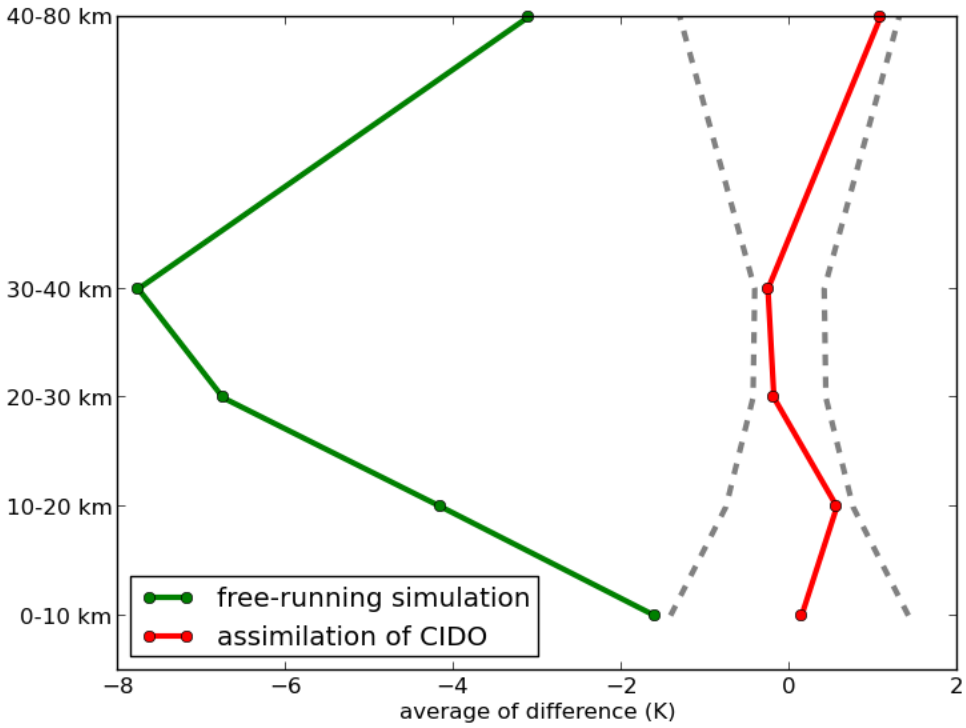


**Figure S1.** Global-time mean temperature difference between MCS observations and the free-running model (green) and CIDO-only reanalysis (red), during MY29 $L_s = 110° - 330°$. Grey dashed lines show the average uncertainty in the MCS observations (Kleinböhl et al., 2009).

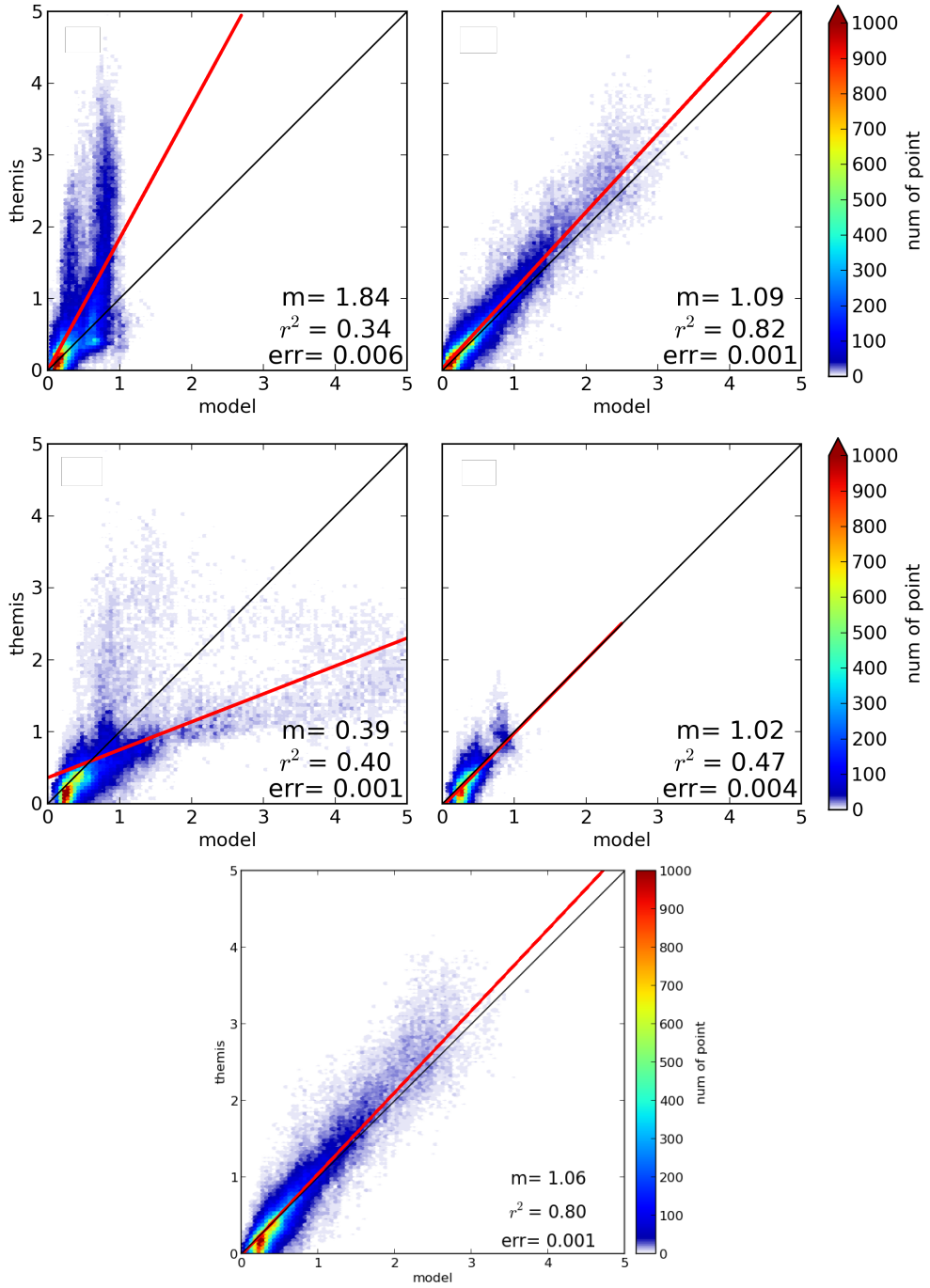


**Figure S2.** Scatter plots showing individual $\tau_{\text{ref}}$ points comparing the assimilated THEMIS observations with the free-running model and various reanalyses over the period shown in Fig. 4 of the main text. Colours show the data density as the number of points per square of side $\tau_{\text{ref}} = 0.05$. Red lines show the linear least square fit, with $m$ the fitting coefficient, $r^2$ the coefficient of determination, and $err$ the standard error in $m$. Black lines show $m = 1$.

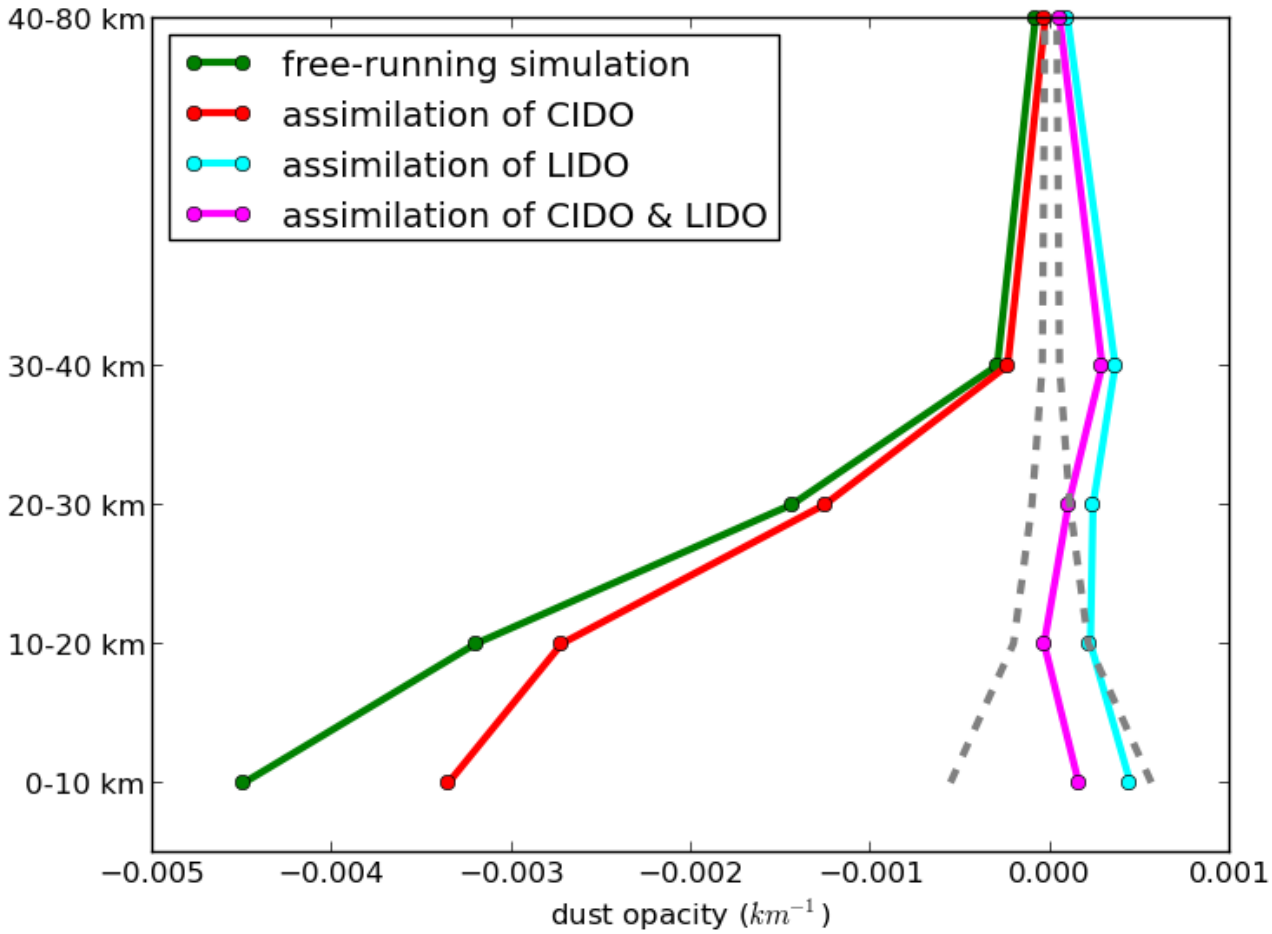


**Figure S3.** Global-time mean dust opacity difference between observed MCS dust opacities and the free-running model (green), CIDO-only reanalysis (red) LIDO-only reanalysis (cyan), and joint CIDO/LIDO reanalysis (magenta), during MY29 $L_s = 110° - 330°$. Grey dashed lines show the average error in the MCS observations.

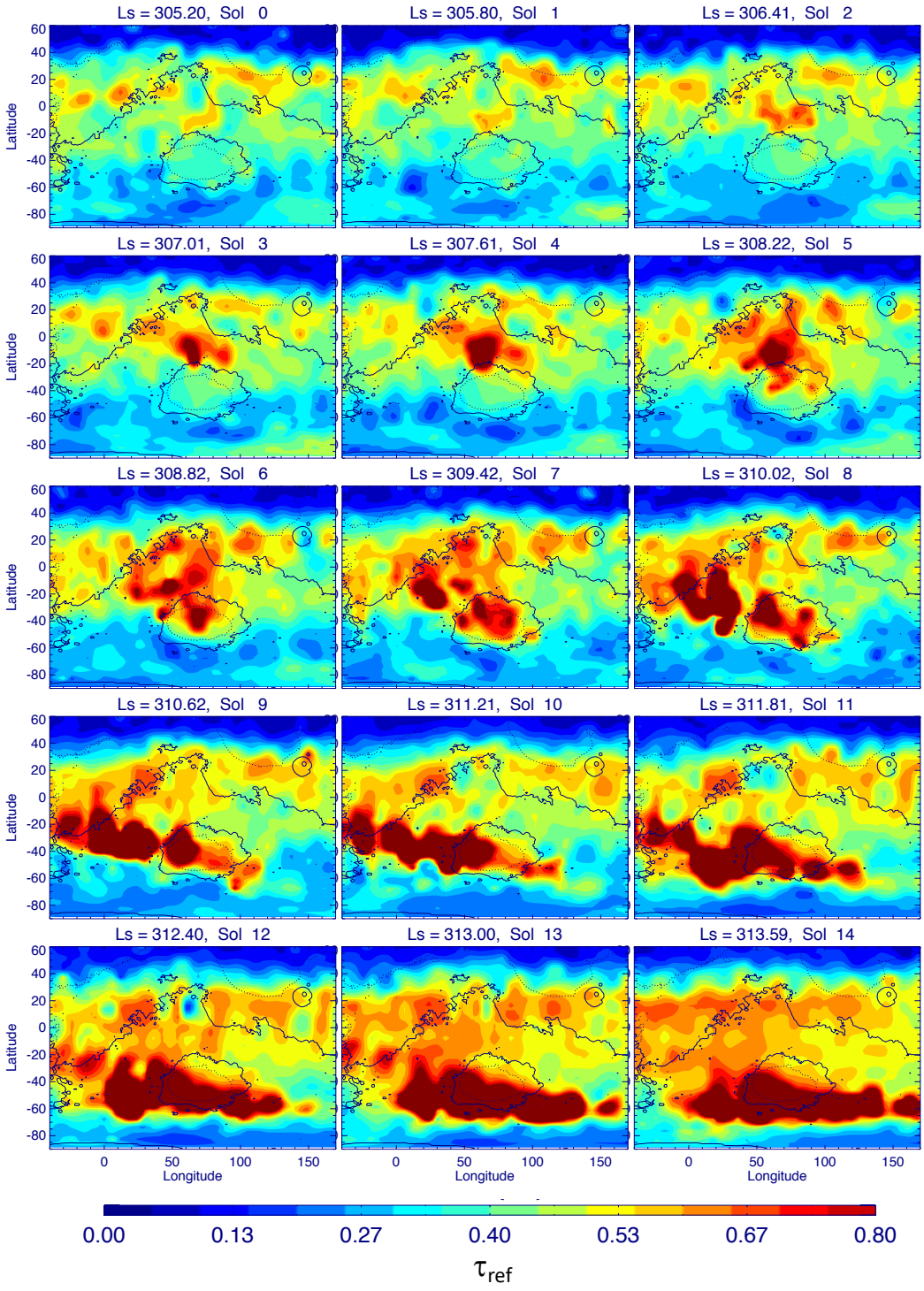


**Figure S4.** Spatial maps of daily column integrated visible dust optical depth $\tau_{ref}$ during the development of a regional dust storm during late southern summer in MY29. Day 0 corresponds to sol 571 of MY29 and the mean $L_s$ for each sol is indicated above each frame. Fields were



obtained by binning and interpolating MCS observations by Montabone et al. (2015) for production of their dust scenarios. Original data provided infrared optical depths which were converted to visible opacities by multiplying by a factor of 2.6 (see text).

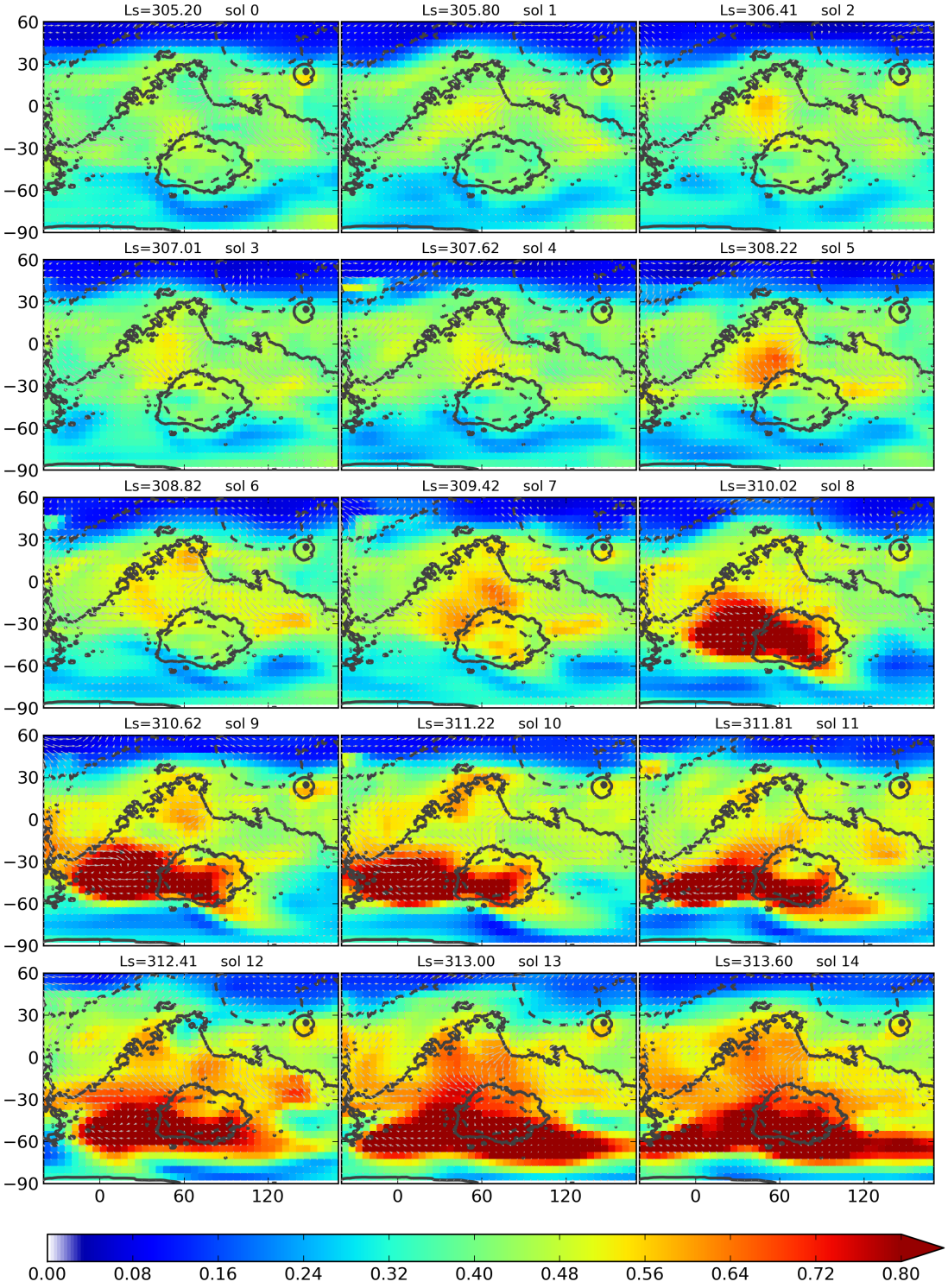


**Figure S5.** Spatial maps of daily averaged column integrated visible dust optical depth $\tau_{ref}$ during the development of a regional dust storm during late southern summer in MY29, obtained using joint CIDO-LIDO dust assimilation, as described in the present work. As for the previous figure, Day 0 corresponds to sol 571 of MY29 and the mean $L_s$ for each sol is indicated above each frame. This illustrates the impact of dust advection within the MGCM in preserving a physically consistent evolution of the dust cloud, compared with simpler binning and interpolation as used in Figure S4.

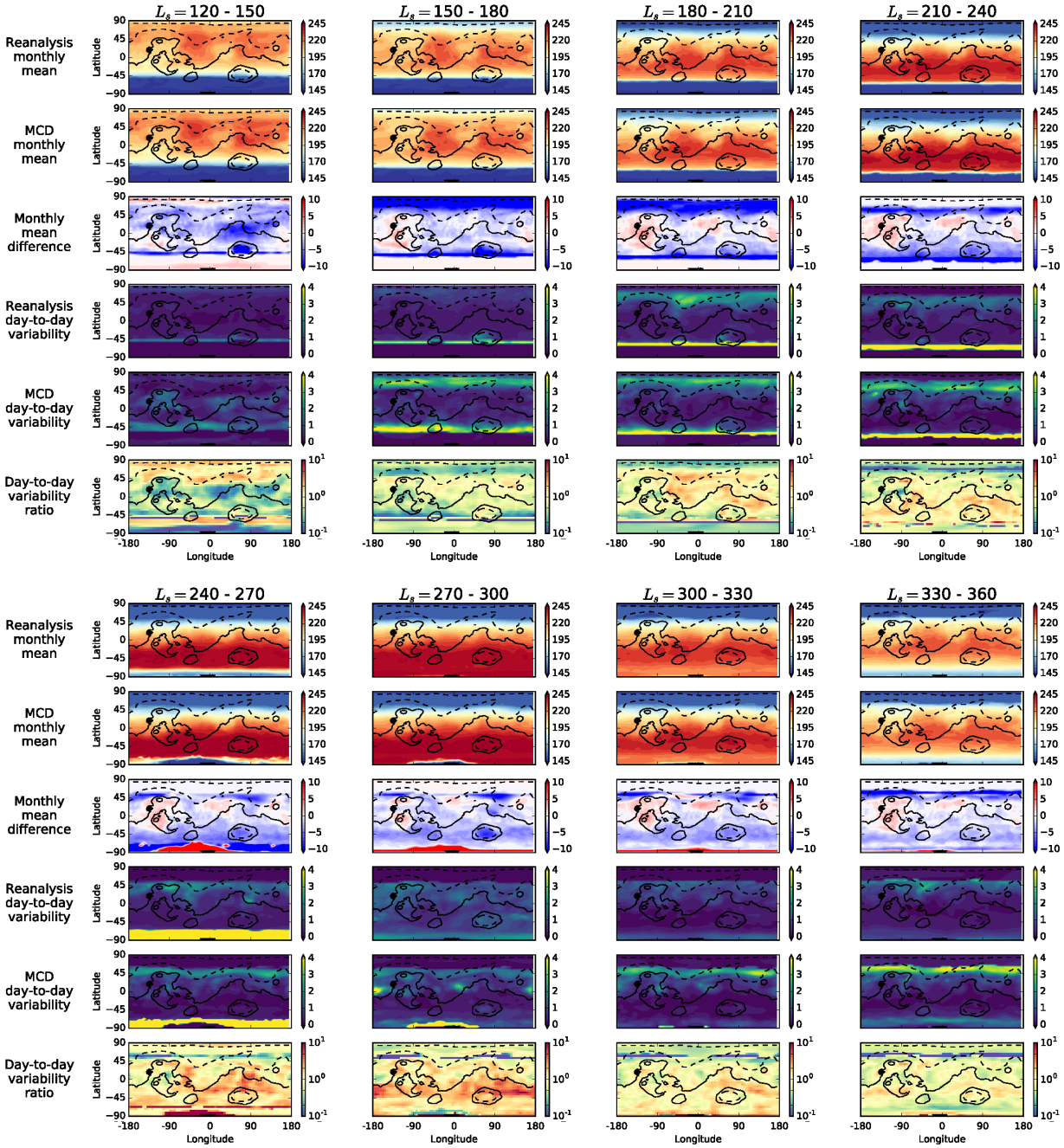


**Figure S6.** Surface temperature during MY28.

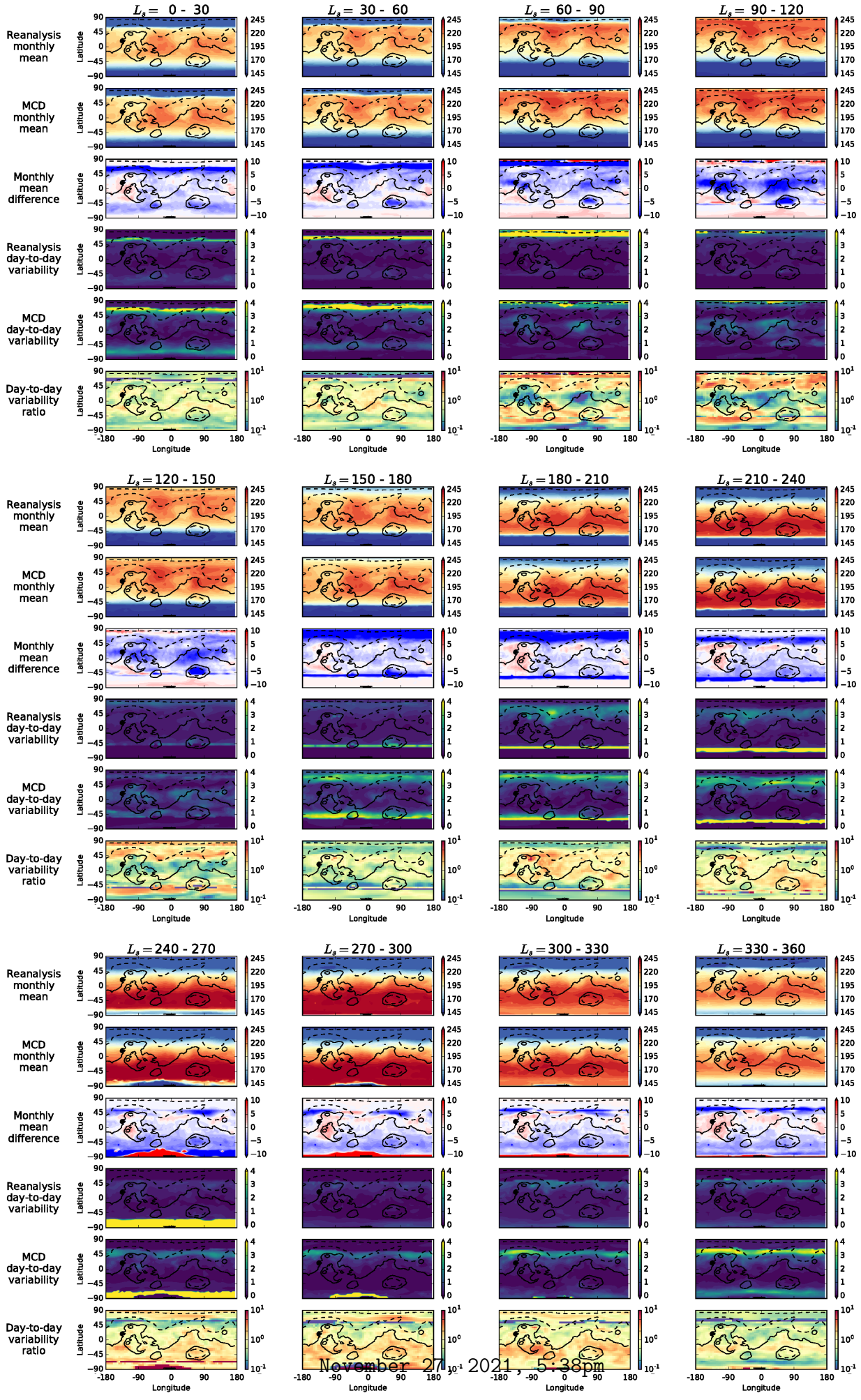


**Figure S7.** Surface temperature during MY29.

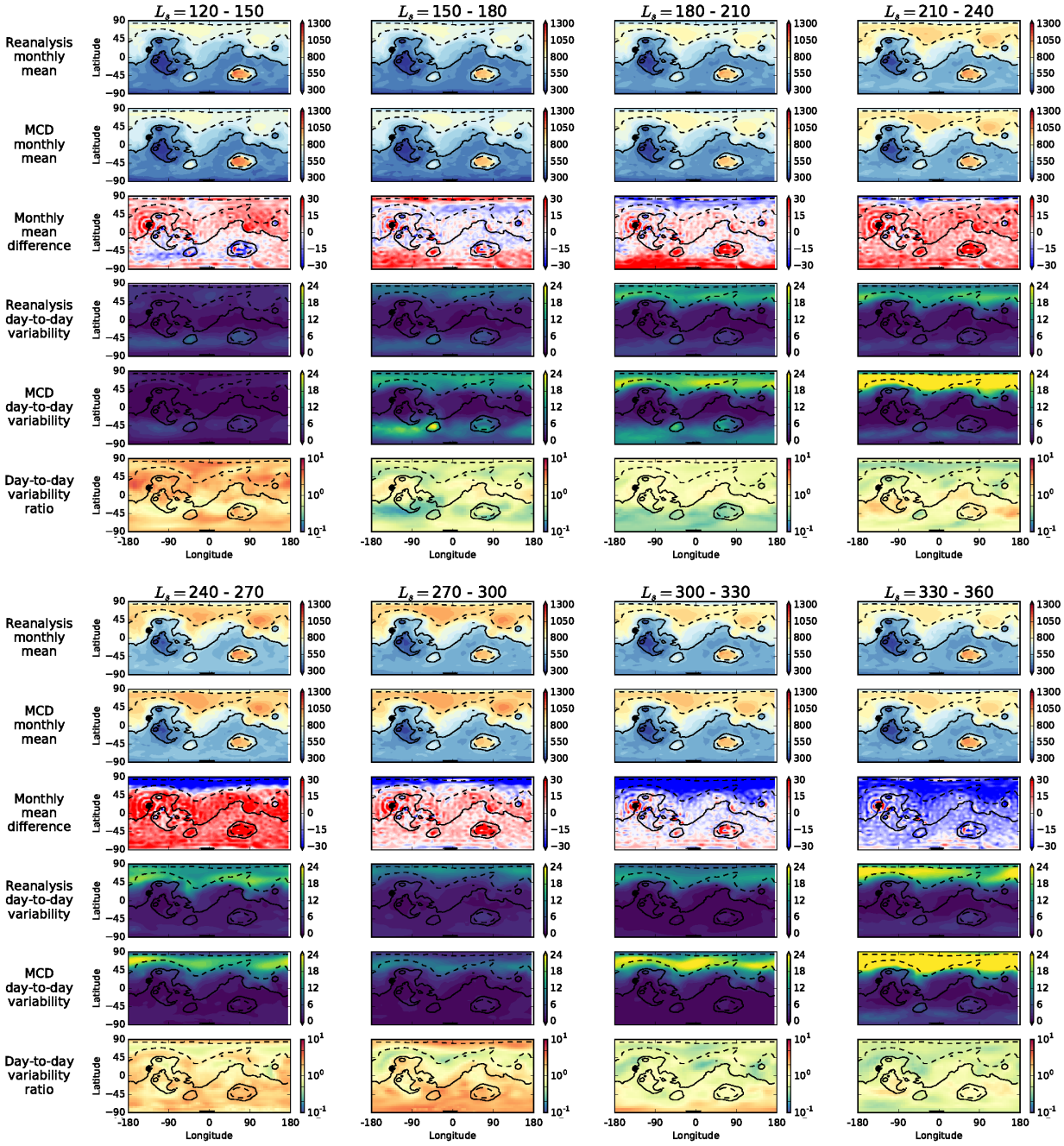


**Figure S8.** Surface pressure during MY28.

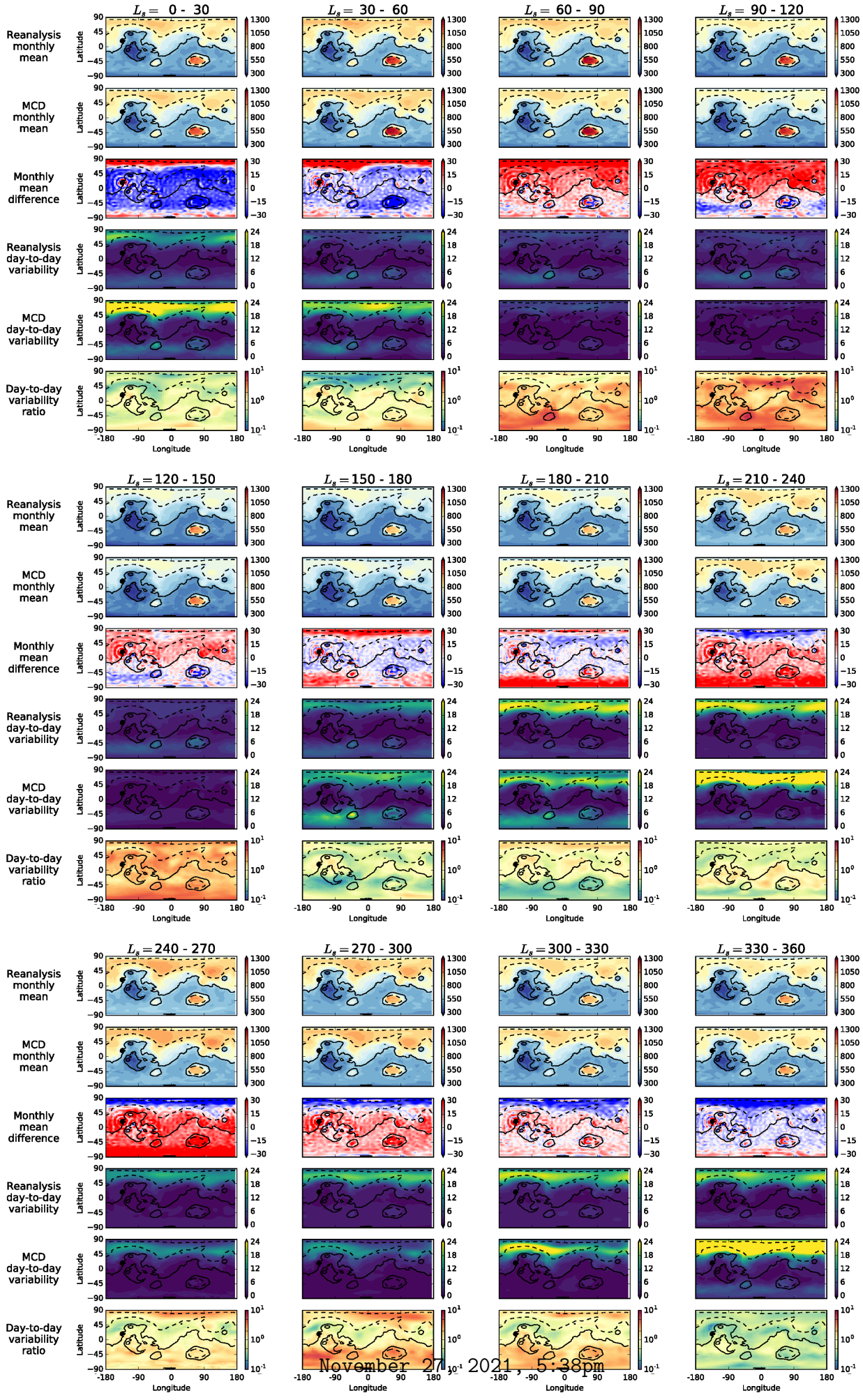


**Figure S9.** Surface pressure during MY29.

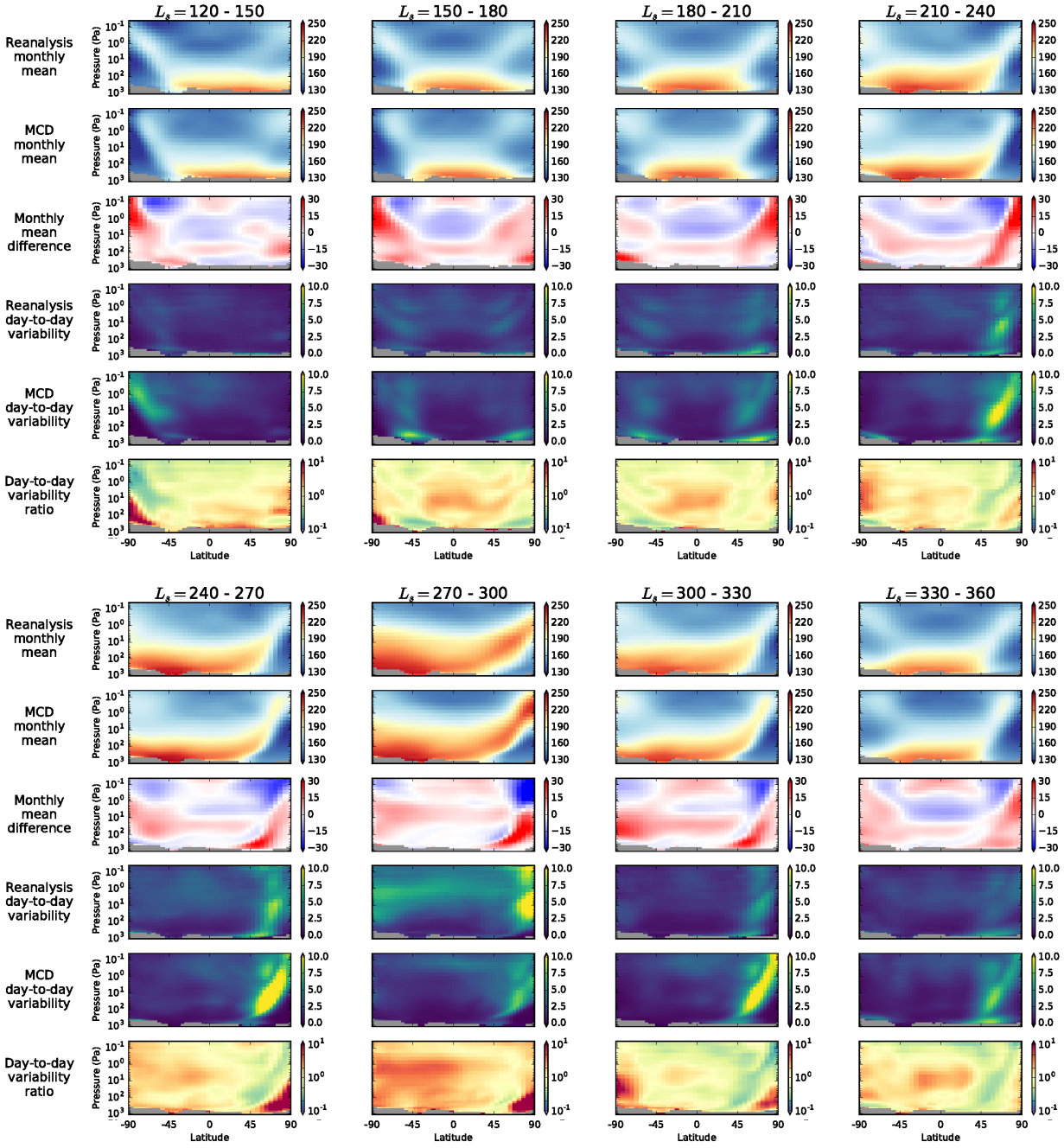


**Figure S10.** Zonal mean temperature during MY28.

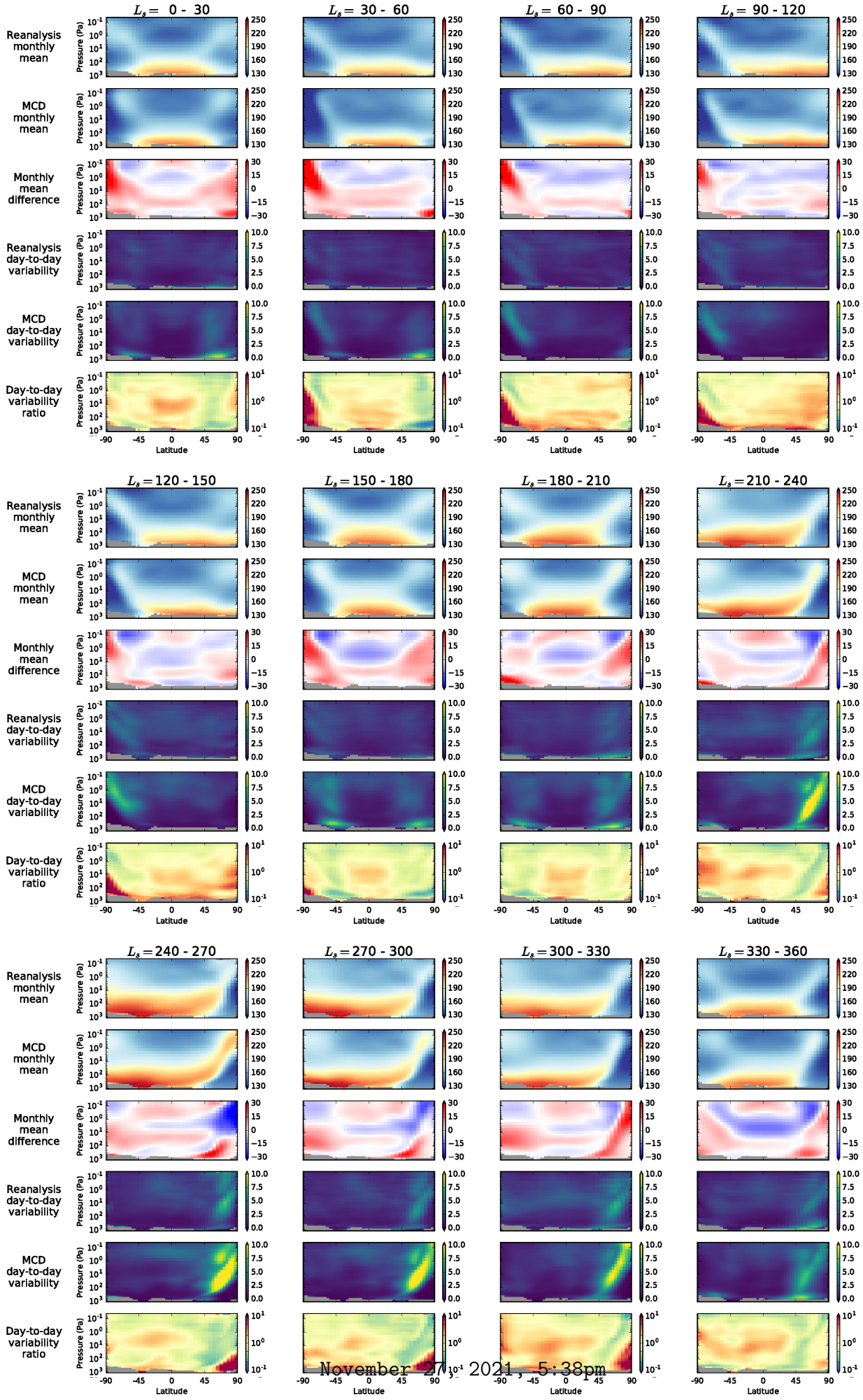


**Figure S11.** Zonal mean temperature during MY29.

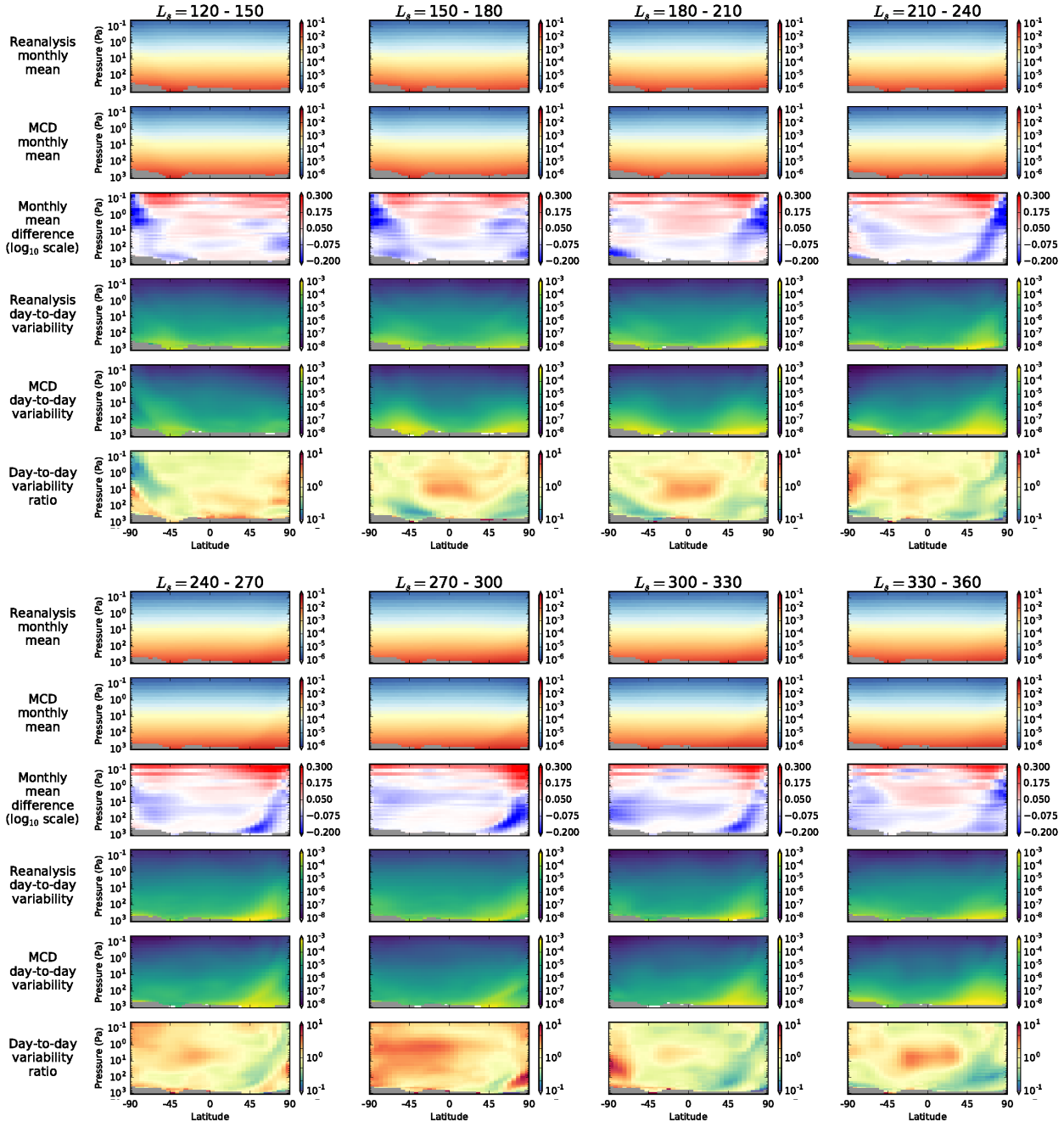


**Figure S12.** Zonal mean density during MY28.

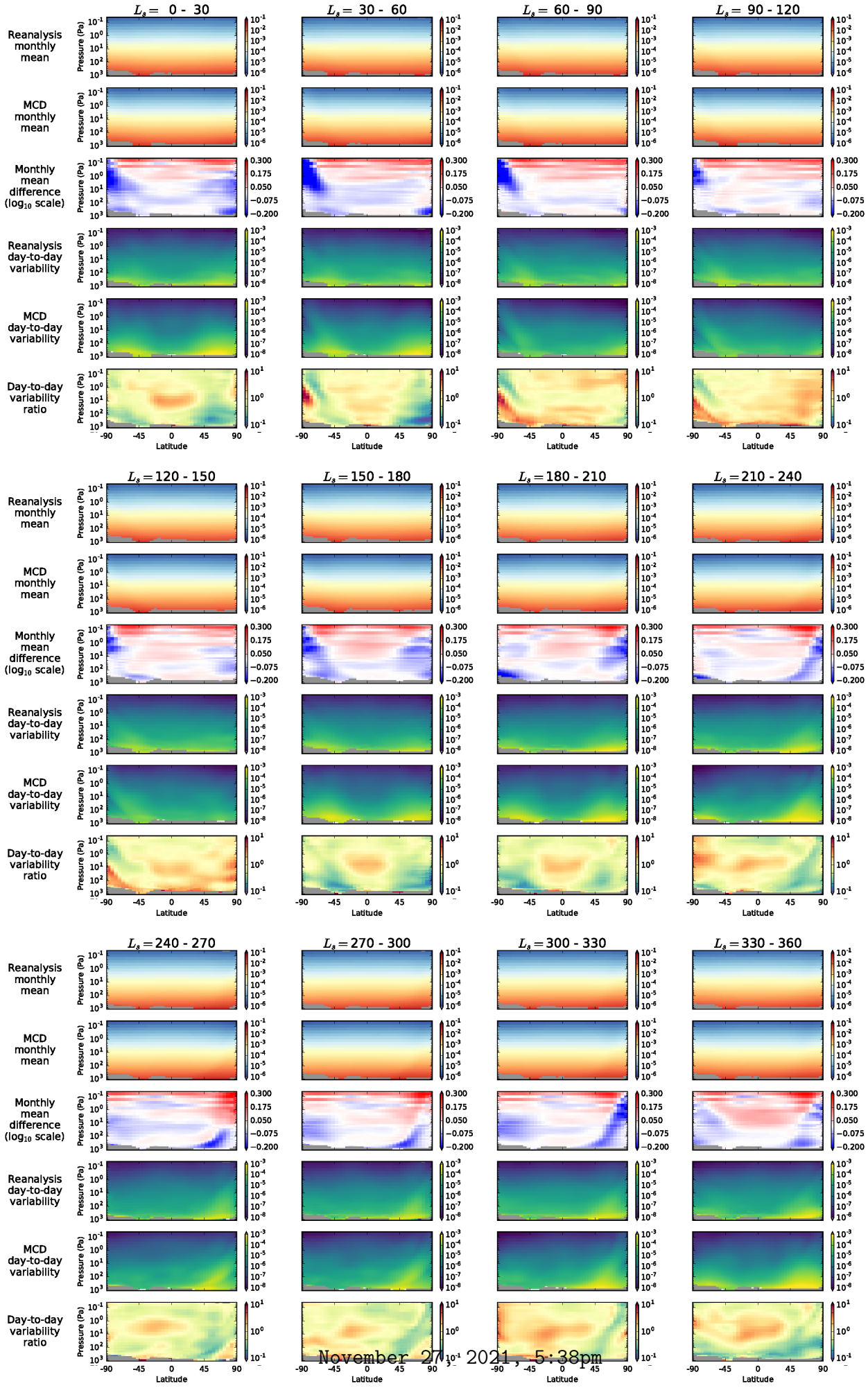


**Figure S13.** Zonal mean density during MY29.

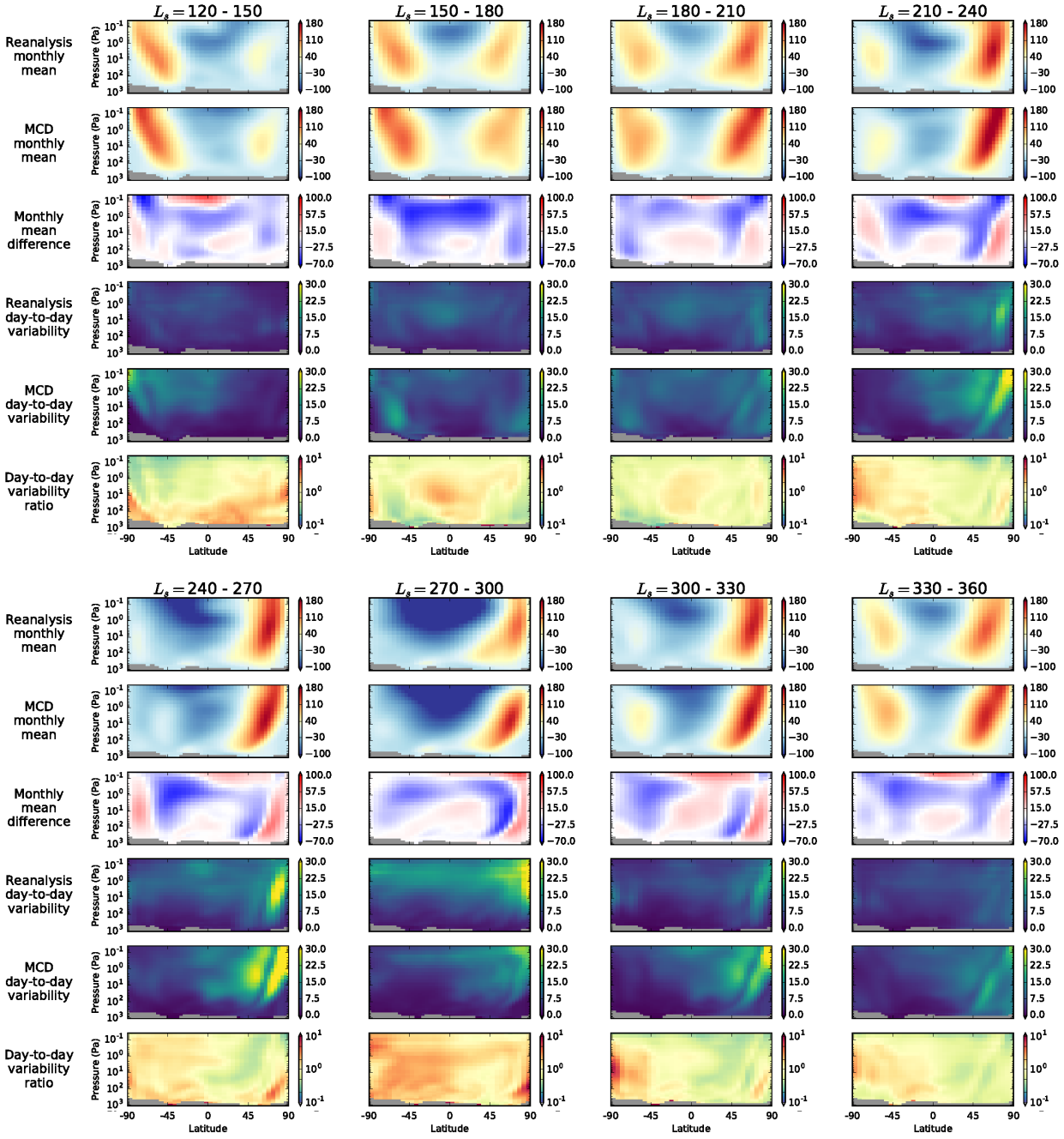


**Figure S14.** Zonal mean zonal velocity during MY28.

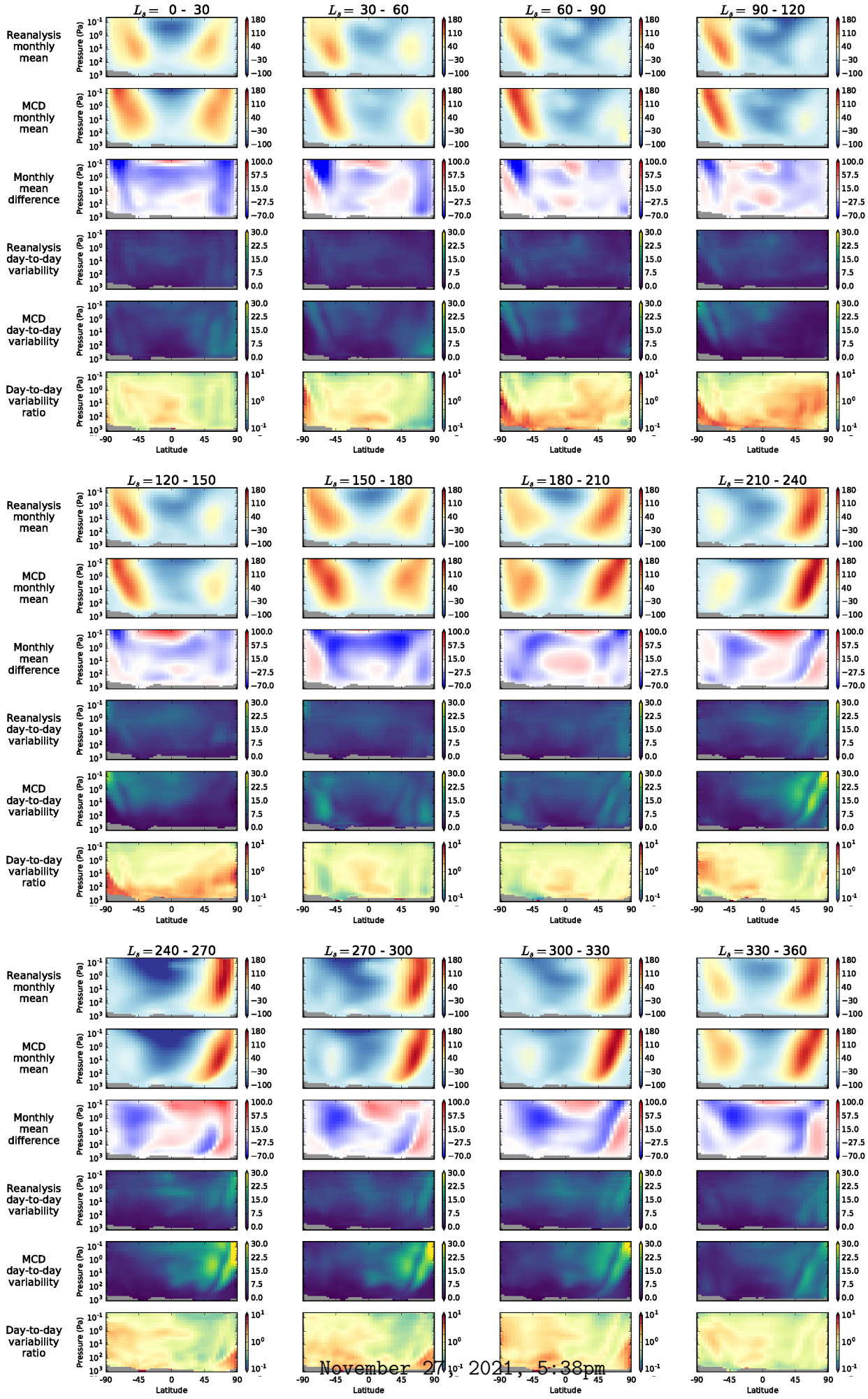


**Figure S15.** Zonal mean zonal velocity during MY29.

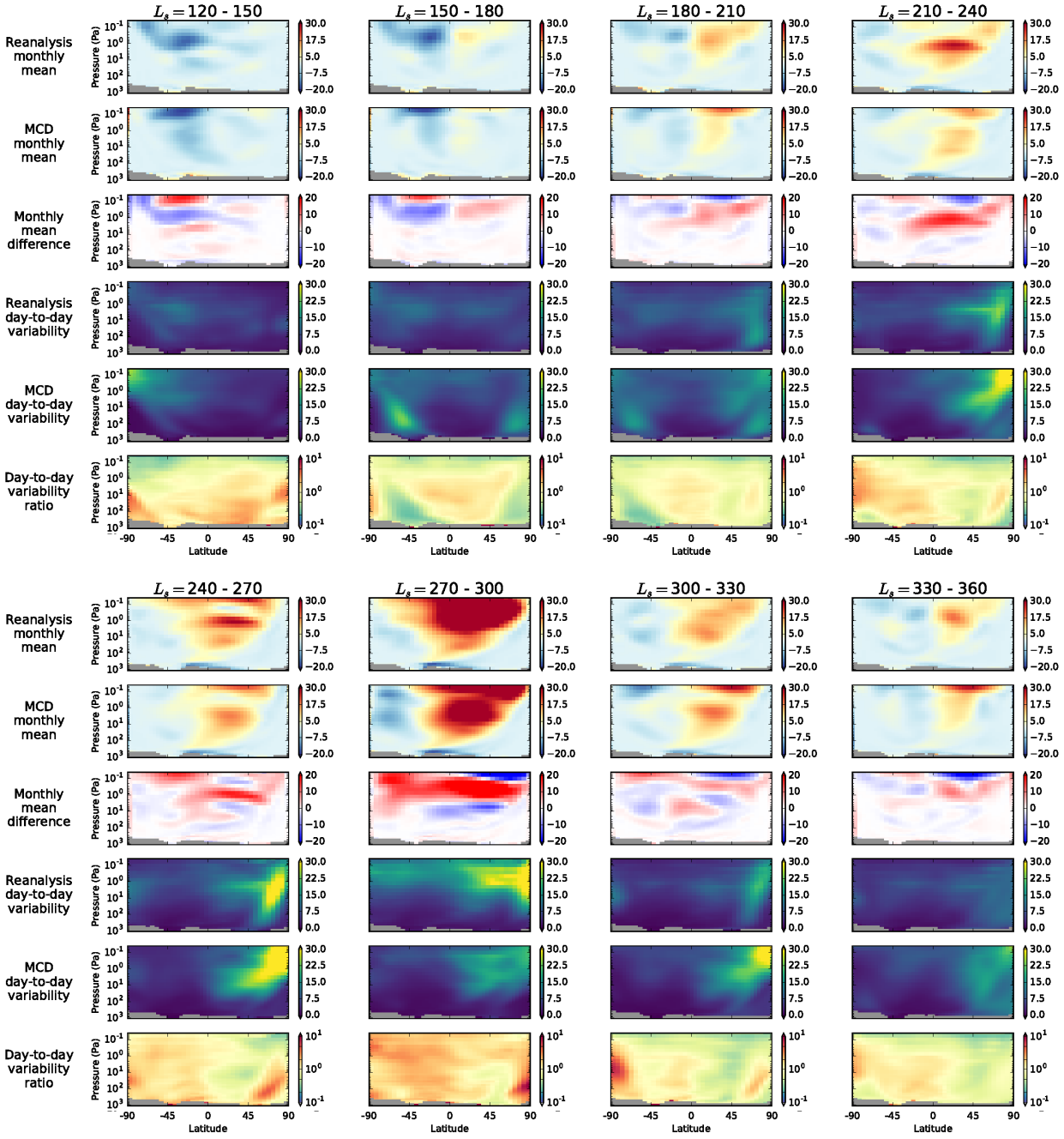


**Figure S16.** Zonal mean meridional velocity during MY28.

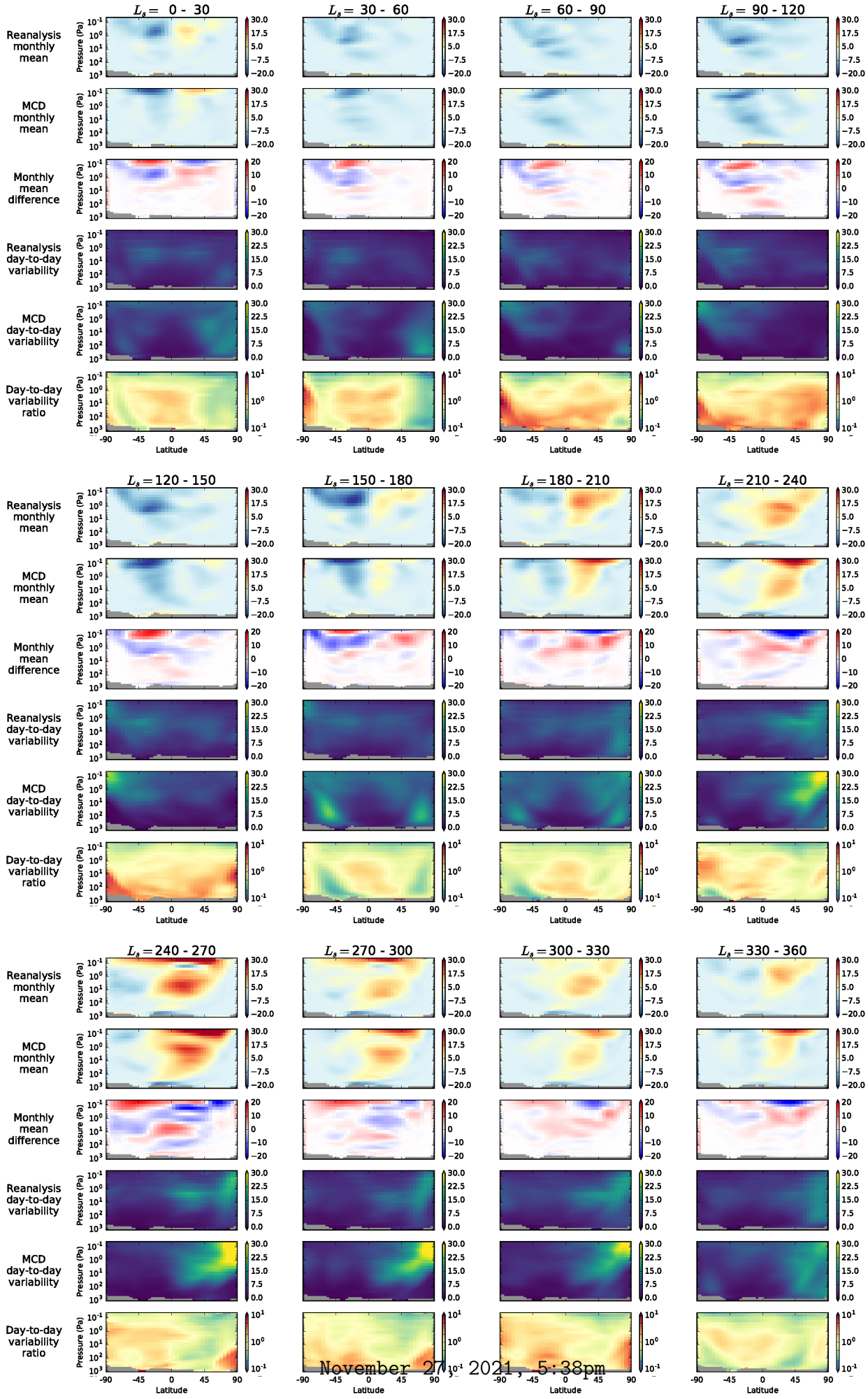




**Figure S17.** Zonal mean meridional velocity during MY29.